CHAPTER SIXTEEN

A Geometric Morphometric Assessment of the Hominoid Supraorbital Region: Affinities of the Eurasian Miocene Hominoids *Dryopithecus*, *Graecopithecus*, and *Sivapithecus*

Kieran P. McNulty

INTRODUCTION

Supraorbital morphology in extant hominoids is typically diagnosed using simple, descriptive labels: a rim in *Hylobates*, a costa in *Pongo*, a torus in the African apes, and superciliary arches in modern humans. Similar terms are

Kieran P. McNulty • Department of Sociology & Anthropology, Baylor University, One Bear Place #97326, Waco, TX 76798-7326.

Modern Morphometrics in Physical Anthropology, edited by Dennis E. Slice.
Kluwer Academic/Plenum Publishers, New York, 2005.

also applied to character states in fossil specimens, though often with a qualifier (e.g., "poorly developed"). While these definitions may be adequate to delineate among extant forms, they provide no objective basis for comparison—among either alternate morphologies or researchers. Moreover, such descriptive diagnoses cannot meaningfully characterize variability within taxa. Thus, the demarcation between one character state and another remains largely a matter of individual preference. For these reasons, verbal description is inadequate for distinguishing among the diverse supraorbital morphologies of fossil apes.

This is particularly evident in the disagreement surrounding Late Miocene hominoids from Eurasia. Based on recent discoveries of *Dryopithecus* (Begun and Moyà Solà, 1992; Kordos, 1987; Kordos and Begun, 2001), a variety of opinions have emerged over the shape of its supraorbital morphology: an incipient torus, indicative of African apes and early humans (Begun, 1992; Kordos and Begun, 2001); a costa, as in *Pongo* (Köhler et al., 2001); or, primitive morphology of great apes (e.g., Andrews, 1992) or even catarrhines (Benefit and McCrossin, 1995). Similar hypotheses have been put forth for the partial cranium of *Graecopithecus*, suggesting that its supraorbital features share affinities with pongines (e.g., Köhler et al., 2001), hominines (i.e., African apes and humans; Begun, 1992; Benefit and McCrossin, 1995), hominins (i.e., members of the human clade; e.g., Bonis and Koufos, 2001), or with *Gorilla* (Dean and Delson, 1992). Such dependence on descriptive labels for supraorbital character states can result in substantial differences in phylogenetic hypotheses (compare, e.g., Begun, 1994; Benefit and McCrossin, 1995; Köhler et al., 2001).

This study used landmark-based morphometrics to quantify morphology and variation in the supraorbital region of extant and fossil hominoids. The goals of this project were to (a) assess the ability of supraorbital morphology to differentiate among modern taxa, (b) determine phenetic affinities of fossil specimens, and (c) examine the affinities of fossil morphologies within a phylogeny of extant hominoids. The much-debated *Dryopithecus* and *Graecopithecus* specimens were included here, as well as the partial face of *Sivapithecus* (GSP 15000). While most authors agree that this latter fossil shares many similarities with *Pongo*, there is disagreement as to whether these are synapomorphies (e.g., Ward and Kimbel, 1983), symplesiomorphies (e.g., Benefit and McCrossin, 1995), or convergently derived (see Pilbeam and Young, 2001).

MATERIALS

Extant hominoid specimens were measured at the American Museum of Natural History, National Museum of Natural History, Museum of Comparative Zoology, Peabody Museum, Powell-Cotton Museum, Humboldt University Museum für Naturkunde, and Musée Royal de l'Afrique Centrale. Only adult, wild-shot (for non-humans) specimens were included. Extant hominoid genera were represented by the following sample sizes: *Gorilla*—70m, 44f; *Homo*—21m, 19f; *Hylobates*—66m, 59f; *Pan*—71m, 91f; and *Pongo*—33m, 39f. Excepting *Hylobates*, all commonly recognized subspecies were sampled; such sampling was rejected for hylobatids due to the multitude of species and subspecies attributed to this genus. Of the four hylobatid subgenera (after Marshall and Sugardjito, 1986), *H*. (*Hylobates*) and *H*. (*Symphalangus*) were included here. The former is represented by three subspecies each of *H. agilis* and *H. muelleri*.

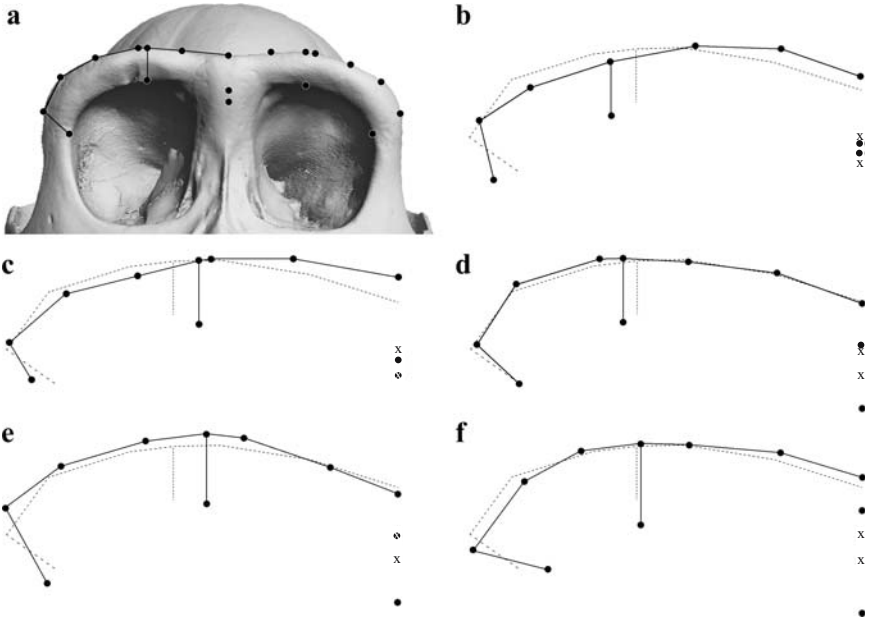

Figure 1. Variation in extant and fossil hominoid supraorbital morphology. (a) Female *Gorilla* cranium showing landmarks used in this study (courtesy of Eric Delson). (b–f) Frontal view of fossil landmark configurations depicting midline and right-side morphology. Fossil landmarks are represented by • connected with solid lines; the overall consensus configuration is shown for contrast using dotted lines and Xs. (b) *Dryopithecus*, RUD 77; (c) *Dryopithecus*, RUD 200; (d) *Dryopithecus*, CLI 18000; (e) *Sivapithecus*, GSP 15000; (f) *Graecopithecus*, XIR 1.

The Miocene Eurasian hominoid sample comprised specimens attributed to *Dryopithecus* (RUD 77, RUD 200, CLI 18000), *Graecopithecus* (XIR 1), and *Sivapithecus* (GSP 15000). Data were collected from original specimens for RUD 77, RUD 200 (Geological Institute of Hungary), and GSP 15000 (in the care of Jay Kelley, University of Illinois College of Dentistry). CLI 18000 and XIR 1 data were collected from high quality casts. Figure 1 illustrates the brow morphology of an extant ape and the landmark configurations of the fossils analyzed in this project. The laser-scan of a female *Gorilla* (Figure 1a) includes the landmarks used for analysis; fossil specimens (Figures 1b–f) are illustrated here by landmarks from the right and midline morphology only, superimposed over the consensus configuration.

METHODS

Data Collection and Processing

Three-dimensional coordinate data were collected using a Microscribe 3DX digitizer (Immersion Corp., San Jose, CA) and recorded in centimeters to four decimal places. The 10 landmarks used to quantify supraorbital morphology are listed and defined in Table 1; abbreviations given there are referred to in subsequent text and figures. To further describe this region, semilandmark data from a single space curve (Dean, 1993; Harvati, 2001; McNulty, 2003; Rohlf

Table 1. Landmark definitions, abbreviations, and intraobserver error

Landmark	Abbreviation	Definition	Side	Mean error (mm)
Frontomalare Temporale	FMT	Intersection of the frontozygomatic suture and the temporal line	RIGHT LEFT	0.23 0.66
Frontomalare Orbitale	FMO	Intersection of the frontozygomatic suture and the orbital rim	RIGHT LEFT	0.24 0.49
Mid-torus Inferior	MTI	Point on the inferior margin of the supraorbital torus at the middle of the orbit	RIGHT LEFT	0.26 0.63
Mid-torus Superior	MTS	Point on superior aspect of the torus directly above mid-torus inferior	RIGHT LEFT	0.37 0.72
Glabella	GLA	Most anterior midline point on frontal bone	MIDLINE	0.46
Nasion	NAS	Most superior point on the internasal suture	MIDLINE	0.52

and Marcus, 1993) were also included. This "line" was represented by a series of closely spaced points collected along the superior border of the supraorbital morphology, bounded by right and left frontomalare temporale. Each curve was then resampled down to nine evenly spaced semilandmarks (L1–L9) for inclusion in analyses.

Ten replicate data series were collected from a single female *Gorilla* cranium to assess the effect of intraobserver error. The mean distance of each replicate landmark to the overall landmark mean was computed to provide an average error estimate for each landmark. These results are given in Table 1. The root mean squared distance of all landmarks to their individual means, computed as the square root of the trace of the covariance matrix, was 0.2 mm.

Of the fossils included here, only RUD 77 completely preserves the relevant morphology. Therefore, missing bilateral landmarks and semi-landmarks were reconstructed by reflecting antimeres across the sagittal plane. Rather than basing such reconstructions on only these few supraorbital landmarks, this procedure was undertaken within the context of a large, comprehensive set of cranial landmarks (see McNulty, 2003 for a detailed overview and discussion of this procedure). For each fossil, mirrored configurations were created by switching the coordinates of bilateral landmark pairs and then multiplying the z-coordinates of all landmarks by -1. Subsequently, each fossil was superimposed (disallowing reflection) with its mirror configuration according to a fit of midline landmarks. Missing bilateral landmarks were then estimated from the corresponding superimposed mirror configurations.

Morphometric Methods

A generalized Procrustes analysis (GPA) performed in *Morpheus et al.* (Slice, 1998) was used to superimpose all landmark configurations (e.g., Dryden and Mardia, 1998; O'Higgins and Jones, 1998; Slice et al., 1996). This is an iterative, least-squares procedure that scales specimens to a unit size, translates them to a common origin, and rotates them to minimize the sum of squared distances across all landmarks and specimens. Because semi-landmarks have fewer degrees of freedom in which to vary, the GPA was performed on landmark coordinates only; space-curve data were transformed through the superimposition matrix of the landmarks. Other approaches to analyzing space curves—requiring different sets of assumptions—have been developed elsewhere (e.g., Bookstein et al., 1999; Dean et al., 1996; Chapters 3 and 4, this volume), but were not used here.

As GPA results in the data being mapped to a curved, non-Euclidean space (Slice, 2001), fitted specimen configurations were projected into a Euclidean space tangent to this at the sample mean (e.g., Dryden and Mardia, 1998). To test the correspondence between coordinates in these spaces, Procrustes distances were regressed against Euclidean distances using *tpsSmall* (Rohlf, 1999). A strong correlation ($r = 0.9999$, slope $= 0.9974$) indicated close unity between these spaces.

ANALYSES AND RESULTS

Phenetic Analyses

Initial phenetic analyses included both principal components analysis (PCA) and canonical discriminant analysis. The former was used both to reduce dimensionality in the dataset and to explore shape variation among specimens, particularly regarding the relationships of fossils to extant clusters. Given that group membership is reliably known for extant ape genera, discriminant analysis was used to examine shape differences among these taxa and to assign fossil specimens to extant genera. Mahalanobis distance estimates generated from the canonical analyses were also used to study hierarchical relationships among taxa.

Principal Components Analysis: A PCA was performed on the covariance matrix of the aligned coordinates. As PCA generates linear combinations of the original variables ordered sequentially to account for the greatest amount of sample variation (Slice et al., 1996), seven eigenvectors with zero variance were dropped from subsequent analyses. PCA was also used to examine the total sample variance in relatively few dimensions (Neff and Marcus, 1980). Table 2 lists the eigenvalue, proportion of variance, and cumulative variance represented by the first 12 (of 57) PCs—accounting for more than 90% of the total sample variance. An analysis of variance (ANOVA) was performed on PC scores to test for statistical significance among genera along each eigenvector; these results are also shown in Table 2. To determine the groups contributing to such differences, pairwise t-tests with a Bonferroni adjustment were performed on the least-squares adjusted means for each genus. T-test results are given in Table 3. Fossil taxa were not included in ANOVAs and t-tests. Although all principal component (PC) axes were examined during analysis, the majority of group differences were represented by the first four eigenvectors. These are discussed in detail below.

Table 2. Summary of PCA and ANOVA results for the first 12 (of 57) eigenvectors[a]

Eigenvector	PCA results			ANOVA results	
	Eigenvalue	Proportion	Cumulative	F value	Pr > F
1	0.01034	0.4168	0.4168	477.89	<0.0001
2	0.00442	0.1783	0.5950	416.76	<0.0001
3	0.00204	0.0824	0.6774	174.22	<0.0001
4	0.00134	0.0544	0.7318	72.09	<0.0001
5	0.00128	0.0518	0.7835	1.52	0.1959
6	0.00100	0.0407	0.8242	10.28	<0.0001
7	0.00057	0.0232	0.8474	3.20	0.0130
8	0.00051	0.0209	0.8683	4.31	0.0019
9	0.00035	0.0145	0.8828	0.97	0.4216
10	0.00034	0.0140	0.8968	2.33	0.0554
11	0.00028	0.0114	0.9081	0.42	0.7915
12	0.00026	0.0106	0.9188	6.37	<0.0001

Note:

[a] PCA results show statistics for the latent roots of the sample variance (eigenvalues), the proportion of variance explained by each component, and the cumulative proportion of the variance summarized by each PC and those preceding it. F-values and probabilities are given for one-way ANOVAs testing the null-hypothesis that all genera share a common mean.

Table 3. T-test results with a Bonferroni adjustment showing the probability that pairs of genera share the same mean on the first 4 (of 57) PCs

	Gorilla	*Homo*	*Hylobates*	*Pan*
PC 1				
Homo	0.0094	—		
Hylobates	<0.0001	<0.0001	—	
Pan	1.0000	0.0226	<0.0001	—
Pongo	<0.0001	<0.0001	<0.0001	<0.0001
PC 2				
Homo	<0.0001	—		
Hylobates	<0.0001	0.0007	—	
Pan	<0.0001	<0.0001	<0.0001	—
Pongo	<0.0001	<0.0001	<0.0001	<0.0001
PC 3				
Homo	<0.0001	—		
Hylobates	<0.0001	0.0482	—	
Pan	<0.0001	0.2183	<0.0001	—
Pongo	<0.0001	1.0000	1.0000	<0.0001
PC 4				
Homo	<0.0001	—		
Hylobates	0.0489	<0.0001	—	
Pan	1.0000	<0.0001	0.0094	—
Pongo	0.0010	<0.0001	<0.0001	0.0007

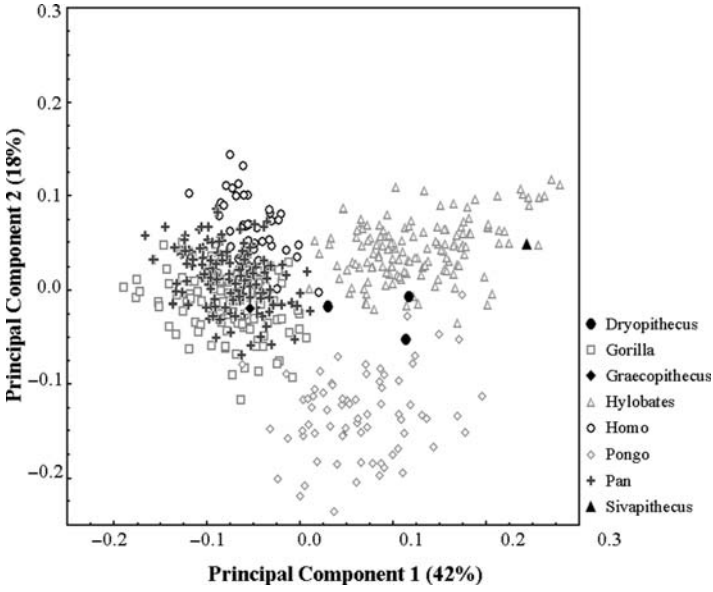

Figure 2. Plot of specimen scores for principal components 1 and 2.

Principal Component One: The first eigenvector summarizes more than 41% of the total sample variation. T-test results indicate significant differences between all pairs of taxa except *Pan* and *Gorilla*. It is clear from a plot of PC scores (Figure 2) that the first PC axis largely separates hominines from *Pongo* and *Hylobates*. Specimens of *Dryopithecus* and *Sivapithecus* fall beyond the hominine ranges on this axis—the latter encompassed only by *Hylobates*. *Graecopithecus*, on the other hand, is situated among the African apes and humans.

Principal Component Two: This second axis summarizes nearly 18% of the total variability. T-tests were significant for all pairs, although the main distinction in this vector (see Figure 2) is between *Pongo* and the other hominoids. Though overlapping slightly with the ranges of other nonhuman primates, this axis clearly demarcates the orangutan morphology. All of the fossil specimens fall amid the hominine–hylobatid ranges, although only GSP 15000 is completely beyond the range of *Pongo*; CLI 18000 falls closest to the mean for *Pongo*.

Principal Component Three: PC 3 represents only 8% of the sample variance and does not separate taxa as well and the first two. The primary distinction is between *Gorilla* and the other apes, as shown by t-test results and a plot of the

PC scores (see Figure 3). Although t-tests indicate other significant differences between genus means, all five ranges overlap along this axis. RUD 77, RUD 200, and GSP 15000 fall closest to the mean score for *Gorilla*; conversely, CLI 18000 and XIR 1 lie near the center of the other hominoid ranges.

Principal Component Four: The fourth PC captures 5% of the sample variation. All pairwise t-tests show significant differences with the exception of *Gorilla–Pan*. Like PC 3, however, this axis does not visually separate genera. The major difference is between humans and the nonhuman apes (see Figure 3). Among fossil taxa, *Dryopithecus* and *Graecopithecus* specimens group with the latter. Alternatively, *Sivapithecus* has the most negative score—beyond even the range of the modern human specimens.

Discriminant Analysis: A canonical discriminant analysis was performed on the nonzero PCs. Unlike PCA, this procedure uses group membership data to maximize the among-group variation relative to the pooled within-group variation (Slice et al., 1996). Thus, it is useful for exploring group differences and is usually preferable to PCA when group membership is reliably known (Neff and Marcus, 1980). Three related goals were accomplished through this analysis. First, canonical axes were used to explore the effectiveness of these data in distinguishing among extant hominoid genera. Second, Mahalanobis D^2

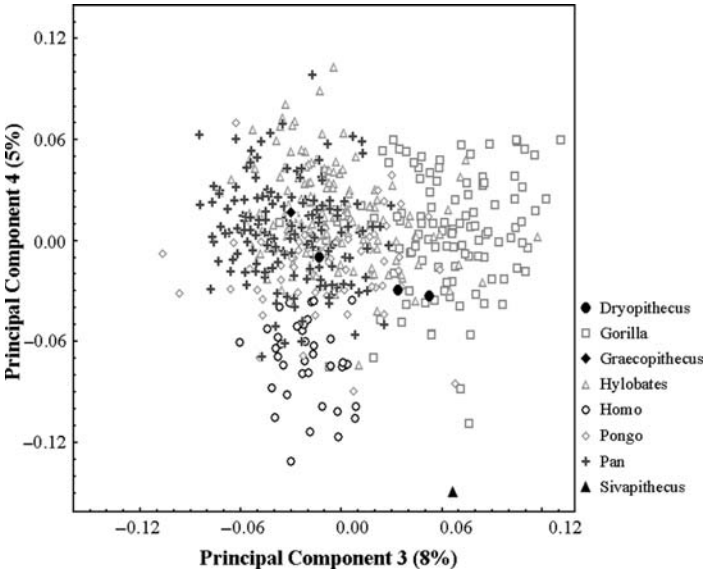

Figure 3. Plot of specimen scores for principal components 3 and 4.

values generated from the analysis were used to compute differences between pairs of genera and to perform a cluster analysis. Finally, the discriminant functions were used to classify fossil specimens into extant genera.

To account for unequal sample sizes among genera, a randomization procedure was also employed. For this, 30 specimens were randomly chosen from each genus and subjected to discriminant analysis. This was repeated 10,000 times, recording cross-validation data, Mahalanobis D^2 values, and fossil classifications. Results of discriminant analyses are discussed below in terms of both the whole-sample analysis and the randomized, equal-sample replicates.

Differences Among Extant Genera: Four canonical axes were computed for the five extant hominoid genera. ANOVAs found highly significant ($p < 0.0001$) generic differences on each; t-tests with a Bonferroni adjustment demonstrated that all pairwise differences were also highly significant ($p < 0.0001$). A cross-validation test was performed to assess the overlap of genus ranges in the canonical space (Neff and Marcus, 1980). This procedure computed the posterior probabilities of correctly reassigning each extant specimen based on discriminant functions calculated from all other specimens. Cross-validation results from both whole-sample and equal-sample analyses are shown in Table 4. Based on the whole sample, all genera scored better than 95% reassignment except *Homo* (92%); mean values for cross-validations in the replicate series were better than 99% in all taxa. Results of ANOVAs, t-tests, and cross-validation tests all indicate that supraorbital morphology is highly robust in discriminating among hominoid genera.

Table 4. Cross-validation results from discriminant analyses[a]

	Whole-sample discriminant analysis					Randomization	
Into	*Gorilla*	*Homo*	*Hylobates*	*Pan*	*Pongo*	Mean	Min.
From							
Gorilla	97.37	0.00	0.00	2.63	0.00	99.78	93.33
Homo	0.00	92.11	0.00	7.89	0.00	99.99	96.67
Hylobates	0.00	0.00	100.00	0.00	0.00	100.00	100.00
Pan	0.60	0.00	0.00	99.40	0.00	99.96	96.67
Pongo	0.00	0.00	0.00	0.00	100.00	100.00	100.00

Note:

[a] Whole-sample results show the percentage of extant specimens from genera on the left that were assigned to genera listed across the top. Randomization results list the mean and minimum percentage of correct reassignments calculated in 10,000 equal-sample replicate analyses. See text for further discussion.

Table 5. Matrix of Mahalanobis D^2 values[a]

	Gorilla	*Homo*	*Hylobates*	*Pan*	*Pongo*
Gorilla	—	66.583	69.256	24.017	74.776
Homo	88.397	—	62.704	30.613	106.546
Hylobates	74.531	74.078	—	42.554	62.395
Pan	25.362	49.828	47.034	—	68.850
Pongo	93.851	134.824	69.980	86.322	—

Note:
[a] Scores in the lower triangle were generated from the whole-sample analysis; mean values from equal-sample replicate analyses are shown in the upper triangle.

Mahalanobis D^2: Mahalanobis D^2 values, with a correction for bias (Marcus, 1969), were generated to estimate the distance in canonical variates space between population centroids (Neff and Marcus, 1980). Table 5 lists D^2 values based on the whole sample (lower triangle) and on average values from the equal-sample replicates (upper triangle). The two sets of numbers cannot be individually compared as they represent differently scaled canonical spaces (Neff and Marcus, 1980). Relative distances among genera ought to be comparable, however, if sample size differences did not impact results. As shown in Table 5, however, distances between *Homo* and the other taxa are significantly reduced when sample size is held equal; this is particularly evident in its distances to *Gorilla* and *Pan*. The difference between whole-sample and equal-sample D^2 values suggests that the sample size of humans used here—markedly smaller than other samples—*does* affect the outcome of these analyses and must be taken into consideration.

Mahalanobis D^2 is also the basis of the multivariate extension of pairwise t-tests, Hotelling's T^2, and follows an F distribution (e.g., Neff and Marcus, 1980). It was used here to evaluate the probability that two population centroids are statistically different across the entire canonical space. Results indicate that all pairwise groups were highly significantly different ($p < 0.0001$)—not surprising, perhaps, in a genus-level analysis.

To visualize distance relationships hierarchically, the unweighted pair-group method using arithmetic averages (UPGMA) was used to cluster genera by D^2 values. Figure 4 shows cluster diagrams based on the whole sample (Figure 4a) and on randomization means (Figure 4b). The cophenetic correlations of both trees are similar at 0.83 and 0.81, respectively. The main difference between them is the clustering of hominines (*Gorilla*, *Pan*, and *Homo*) in the replicate

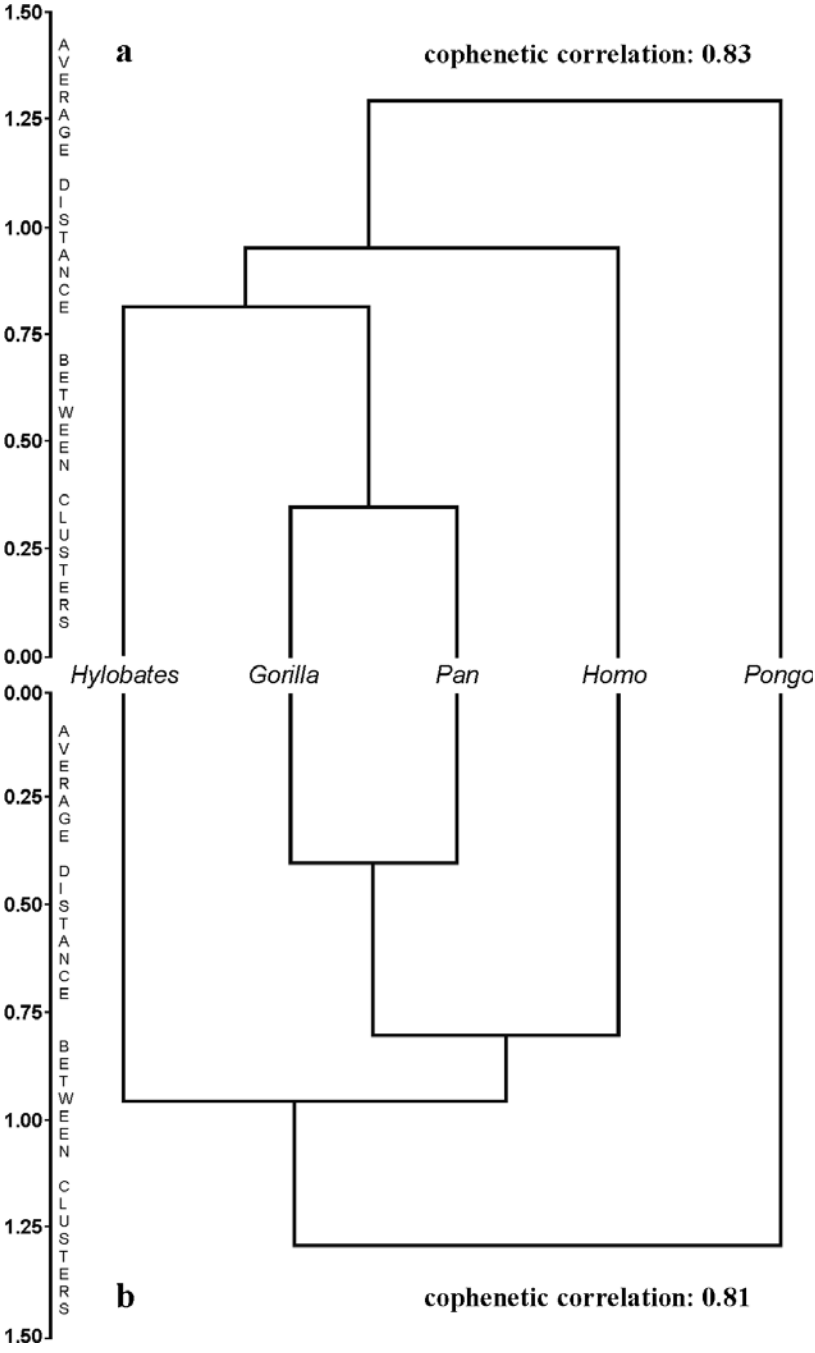

Figure 4. UPGMA cluster diagrams based on (a) Mahalanobis D^2 values from the entire sample of specimens, and (b) mean Mahalanobis D^2 values from 10,000 equal-sample replicates.

series. This again suggests that the smaller sample of *Homo* specimens affects the outcome of these analyses.

As the cophenetic coefficients demonstrate, the UPGMA amalgamation criterion distorts the distances between taxon pairs. It is useful, therefore, to consider cluster results conjointly with the D^2 matrix (see Table 5). The similarity of *Gorilla* and *Pan* is manifest in both matrix and phenogram. The next closest pair is *Pan–Hylobates* (whole-sample) or *Pan–Homo* (randomization). The latter pairing is more likely to be accurate, as it derives from analyses of equal-sample sizes (Neff and Marcus, 1980). In either case, however, their clustering with the *Gorilla–Pan* group is driven by similarities to *Pan*, rather than *Gorilla*. Indeed, *Homo* and *Hylobates* are marginally more similar to each other than either is to *Gorilla*. It is interesting to note that, in both whole-sample and equal-sample analyses, *Homo* was most similar in morphology to *Pan*; indeed, in the replicate series, the difference between *Pan* and *Homo* was only marginally greater than that between the two African apes. Thus, while evolutionary expansion of the brain has dramatically altered the outward appearance of human supraorbital morphology, the actual configuration of landmarks in this region seems largely unaltered (see also McNulty, 2003). *Pongo* is most similar to *Hylobates* in canonical space. Its overall D^2 values, however, indicate that its morphology is substantially different from those of other extant hominoids.

Fossil Assignments: Discriminant functions computed above were also used to assign fossil specimens to extant genera. Table 6 lists the posterior probabilities of grouping fossils in each genus, the percentage of assignments from replicate analyses, and the single resulting classifications. Among *Dryopithecus* specimens, RUD 200 shows strong affinities to *Gorilla*; probabilities of classifying it in other genera were negligible in both whole-sample and equal-sample analyses. RUD 77 was assigned to *Hylobates*, but with only a 92% probability from the whole sample analysis; when sample size is controlled, RUD 77 was placed within *Hylobates* only marginally more often than in *Pan*. CLI 18000 grouped among hylobatids with much stronger support ($p = 0.9997$) in the whole-sample analysis; in the randomization procedure, it grouped with *Hylobates*, *Gorilla*, and *Pan* 58%, 21%, and 15% of the time, respectively. Importantly, none of the *Dryopithecus* specimens demonstrated any affinity to *Pongo*. Results for XIR 1 were unambiguous, placing it with *Gorilla* in all analyses. Of the five fossils analyzed here, only GSP 15000 demonstrated any similarity to *Pongo*. The probability of its assignment to any other genus was

Table 6. Fossil assignments based on discriminant analyses of extant genera[a]

Specimen	*Gorilla*	*Homo*	*Hylobates*	*Pan*	*Pongo*	Assignment
RUD 200	1.0000	<0.0001	<0.0001	<0.0001	0.0000	*Gorilla*
	96.92%	0.46%	1.42%	0.21%	0.99%	
RUD 77	<0.0001	<0.0001	0.9183	0.0817	<0.0001	*Hylobates*
	13.39%	13.87%	35.32%	32.12%	5.3%	
CLI 18000	<0.0001	<0.0001	0.9997	<0.0001	<0.0001	*Hylobates*
	20.86%	6.24%	57.81%	14.57%	0.52%	
XIR 1	1.0000	<0.0001	<0.0001	<0.0001	<0.0001	*Gorilla*
	96.84%	0.36%	1.44%	0.24%	1.12%	
GSP 15000	<0.0001	<0.0001	<0.0001	<0.0001	1.0000	*Pongo*
	0.02%	6.06%	14.26%	4.17%	75.49%	

Note:
[a] The first line for each specimen lists results from the whole-sample analysis, including posterior probabilities of grouping with each extant genus and the final discriminant assignment for the fossil. The second line shows the distribution of assignments from 10,000 equal-sample replicate discriminant analyses.

highly unlikely ($p < 0.0001$) from the whole-sample results. In replicate analyses, *Sivapithecus* showed a slightly broader distribution among genera, but still grouped with *Pongo* 75% of the time.

Phylogenetic Node Discrimination

To interpret these data within an evolutionary framework, phylogenetic node discriminations were also undertaken (McNulty, 2003). The fragmentary nature of fossils has made it commonplace for some authors (e.g., Andrews, 1992) to perform cladistic analyses on extant taxa and then place fossils among the resulting branches according to their preserved features. Phylogenetic node discrimination is a morphometric analog to this approach. Given a phylogeny of extant forms (see, e.g., Figure 5), each node in the branching pattern can be treated as a two-group discrimination between taxa on the left branch and taxa on the right. Based on this series of analyses, determined by the assumed phylogeny, one can test the efficacy of extant morphology in delineating branches at each node. In addition, fossil specimens can be tested for membership along each branch. In this manner, one can examine the affinities of fossil specimens to the extant morphologies that comprise the assumed phylogenetic divisions.

Most authors (e.g., Begun et al., 1997; Collard and Wood, 2000; Pilbeam and Young, 2001; Ruvolo, 1994; but see, e.g., Schwartz, 1987) agree on the phylogenetic relationships of extant hominoids (Figure 5), although the

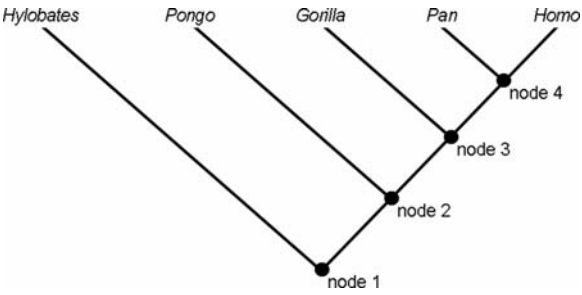

Figure 5. Consensus phylogeny of extant hominoids. Nodes are referred to in the text.

configuration of hominines shown here is better supported from molecular rather than morphological data. Nevertheless, this consensus constitutes a reasonable hypothesis upon which to base node discriminations. Because of substantial differences in sample sizes, a randomization procedure similar to that described above was also used here. In this case, however, random samples were drawn from the two groups defined by each node, rather than from every genus. Table 7 lists the mean cross-validations and fossil assignments that resulted from node discriminations. In all cases, cross-validation scores demonstrated a clear distinction between clades. Fossil assignments are discussed below. Shape differences that correspond to these bifurcations are discussed in detail by McNulty (2003). Those features relevant to the fossils studied here, however, are described below.

Node 1 Analysis: Node 1 separates the hylobatids from the hominids. Among *Dryopithecus* fossils, RUD 200 shows strong support for placement along the hominid lineage. RUD 77 is less well supported here, grouping with hominids only 60% of the time; results for CLI 18000 were equivocal. XIR 1 has the strongest support (89%) among these fossils for clustering with the hominids. Interestingly, GSP 15000 groups most often with hylobatids at a frequency of 68%.

Node 2 Analysis: Node 2 separates the pongines from the hominines. As has been demonstrated here (e.g., Table 5; Figure 4) and elsewhere, however, the supraorbital morphology of *Pongo* is unique among extant apes, and may not represent a reasonable "outgroup" for the hominines. Therefore, node 2 analyses were also run between hylobatines and hominines. Results of the pongine–hominine discrimination demonstrate overwhelming support for grouping all three *Dryopithecus* specimens with the latter. In the hylobatine–hominine

Table 7. Results of phylogenetic node discriminations[a]

	Node 1		Node 2 (*Pongo*)		Node 2 (*Hylobates*)		Node 3		Node 4	
	Hylobatid	Hominid	Pongine	Hominine	Hylobatine	Hominine	*Gorilla*	*Pan–Homo*	*Pan*	*Homo*
% Reclassified correctly	99.98	99.82	100.00	100.00	100.00	100.00	100.00	100.00	100.00	100.00
RUD 200	16.48	83.52	4.30	95.70	17.12	82.88	57.28	42.72	65.02	34.98
RUD 77	39.39	60.61	7.34	92.66	38.46	61.54	49.54	50.46	51.39	48.61
CLI 18000	51.47	48.53	1.13	98.87	80.20	19.80	46.78	53.22	52.77	47.23
XIR 1	11.37	88.63	3.84	96.16	11.35	88.65	67.54	32.46	75.84	24.16
GSP 15000	67.84	32.16	91.92	8.08	58.75	41.25	45.43	54.57	30.08	60.92

Note:

[a] The first row lists the mean percentage of extant specimens correctly reassigned in 10,000 replicate cross-validations for each node discrimination. Subsequent rows show the percentages at which fossil specimens were assigned to branches deriving from each node. Node 2 analyses were run between both pongines and hominines, as well as hylobatines and hominines. See text for further discussion.

analysis, however, only RUD 200 retained this support: RUD 77 ground weakly with hominines and CLI 18000 grouped with *Hylobates* in 80% of the replicates. *Graecopithecus* was strongly supported as a hominine in both analyses. *Sivapithecus* was well supported among pongines (92%), but only marginally placed with hylobatines (59%) in their respective analyses.

Node 3 Analysis: Node 3 separates *Gorilla* from the *Pan–Homo* clade. All three specimens of *Dryopithecus* split among these clades nearly evenly; RUD 200 showed the most distinction, grouping with *Gorilla* in 57% of the cases. Such balanced results, however, indicate that these fossils do not share specific morphology with either clade. XIR 1 shows more differentiation, classifying with *Gorilla* 68% of the time. Like *Dryopithecus*, GSP 15000 showed no particular affinity with *Gorilla* or the *Pan–Homo* group.

Node 4 Analysis: Node 4 separates *Pan* from *Homo*. Given the results from node 3, it would be unlikely to find that these fossils placed strongly in either clade. Both RUD 77 and CLI 18000 demonstrate this, dividing evenly between *Pan* and *Homo*. RUD 200 shows more distinction, grouping with *Pan* in 65% of the replicates. XIR 1 has the strongest support here of any fossil, classifying with *Pan* 75% of the time. GSP 15000, unlike the other fossils, groups more closely with *Homo*, though at a fairly low frequency (61%).

DISCUSSION

It is clear from the above analyses that supraorbital morphology, as captured by the landmarks used here, is very robust in distinguishing among extant hominoids. This is true even in PCA, but particularly evident from the cross-validation and Hotelling's T^2 computed from discriminant analysis. Looking at Mahalanobis D^2 scores and the UPGMA cluster, these data generally support three descriptive character states typically ascribed to hominoid supraorbital morphologies: *Gorilla* and *Pan* share very similar features, with *Hylobates* and *Pongo* distinct from them and each other. A separate character state for *Homo* is not supported here, however, given its affinity to *Pan* (see also McNulty, 2003). The morphology of *Pongo* is most distinct, having the largest D^2 values in both whole-sample and randomization analyses. Beyond providing quantitative support for delineating among extant morphologies, these analyses provided statistical methods for testing the placement of fossil specimens. Figure 6 illustrates some of the shape differences associated with these fossil assignments (see discussion below).

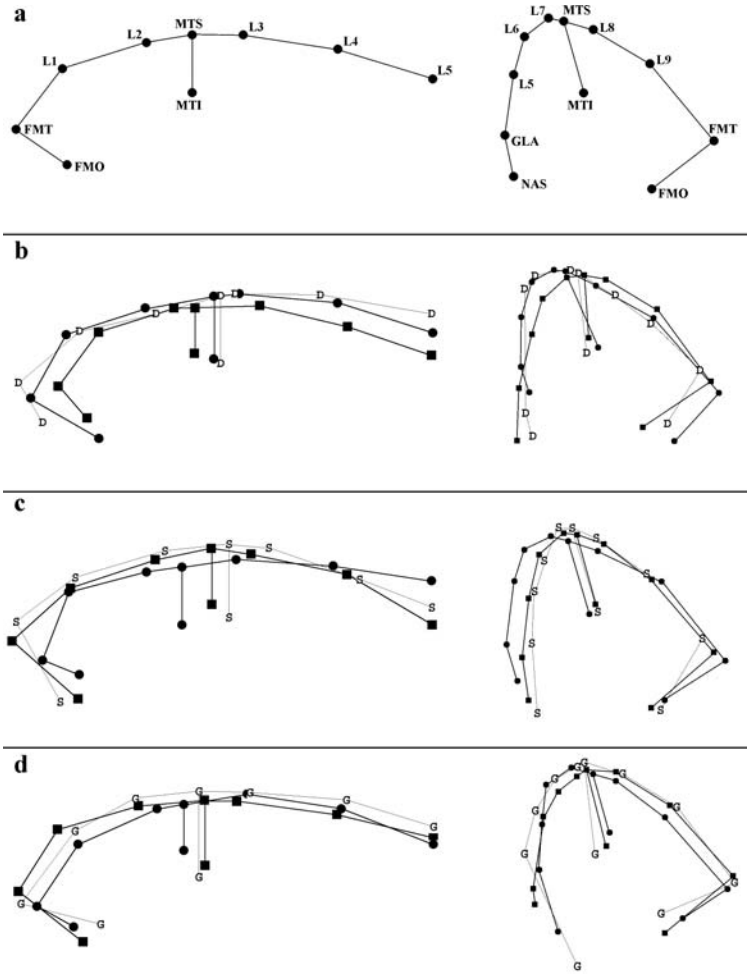

Figure 6. Frontal and lateral views of shape differences between phylogenetic nodes 1–3, with fossil specimens superimposed to illustrate the results of node discriminations. (a) Consensus configuration with landmarks (see Table 1) and semilandmarks (L1–L9) labeled; (b) node 1: ■ = hylobatid, ● = hominid, **D** = RUD 200; (c) node 2: ■ = pongine, ● = hominine, **S** = GSP 15000; (d) node 3: ■ = *Gorilla*, ● = *Pan-Homo*, **G** = XIR 1.

Dryopithecus

The most salient conclusion emerging from analyses of *Dryopithecus* is that these three specimens are not monomorphic. In particular, results for CLI 18000 were substantively different from those of RUD 77 and RUD 200 (see Figure 1). The Spanish specimen was most similar to hylobatids in all analyses.

Results of the replicate discriminant analyses, however, suggest that this is probably not indicative of a close affinity: among extant genera, it grouped with *Hylobates* only 58% of the time. It is possible that the differences between CLI 18000 and the Hungarian specimens represent species-level or even higher taxonomic distinction (see Cameron, 1999). Indeed, these CLI 18000 results might be expected for a stem hominid (e.g., Andrews, 1992) that does not share any particular features with extant apes. Alternatively, one must also consider the possibility that such results reflect poor specimen preservation in the fossil. While this specimen was assumed to retain the entire left zygomatic process of the frontal (Begun, 1994; Moyà Solà and Köhler, 1995), it is possible that the lateral termination is a break rather than a suture. If so, morphometric data from this specimen would be incomparable to those of other specimens.

RUD 200 showed the greatest affinity to hominines. Genus-level discriminant analyses strongly linked this specimen to *Gorilla*. In node discriminations, it closely tracked African apes and humans at the first two nodes and grouped with *Gorilla*—albeit marginally—at node 3. RUD 77 also demonstrated hominine affinities, though not as strongly. The whole-sample analysis assigned this specimen to *Hylobates*; correcting for unequal sample sizes, however, placed RUD 77 in *Hylobates* and *Pan* at similar frequencies. Moreover, RUD 77 favors hominids (60%) to *Hylobates* at node 1, and hominines (61%) to *Hylobates* at node 2. These results add some support to Begun's (e.g., 1994) diagnosis of the *Dryopithecus* brow as a torus. Additional work by McNulty (2003), however, has suggested that the node 2 results shown here may reflect differences in *Dryopithecus* from the pongine and hylobatine morphologies, rather than strong affinities to the hominine form. As such, the Hungarian *Dryopithecus* brows my represent stem hominid morphology.

Figure 6b illustrates, in frontal and lateral views, the differences between hylobatids and hominids at node 1. Superimposed over these is the RUD 200 configuration. As demonstrated by discriminant analyses at node 1, this fossil is most similar to the hominid morphology. In frontal view, the *Dryopithecus* and hominid space curves are fairly consistent in both contour and scope; they differ from the hylobatid in being superiorly placed relative to the orbital rim and the fronto-malar suture, and in their reduced inferior displacement of the midline space curve (L5). Both configurations show thicker brows relative to the hylobatid, with mid-torus landmarks (MTI, MTS) medially placed. While RUD 200 bears some resemblance to the hylobatid in lateral morphology, this frontal view is somewhat misleading. Considering both frontal and lateral aspects,

it is clear that the hylobatid fronto-malar suture is narrow medio-laterally and broader antero-posteriorly, the hominid is broad medio-laterally and narrow antero-posteriorly, and the *Dryopithecus* suture is narrow in both dimensions. In lateral view, RUD 200 and hominid profiles are quite similar, excepting the substantial distance in the former between glabella (GLA) and L5. They contrast with the hylobatid profile, which slopes posteriorly immediately superior to glabella.

Perhaps the most important conclusion one can draw regarding hypotheses for *Dryopithecus* is that none of these specimens demonstrated an affinity to *Pongo*. In the whole-sample analysis, the probability of any *Dryopithecus* specimen grouping with *Pongo* was less than 0.0001; replicate analyses grouped RUD 77 with the orangutans only 5% of the time—the other specimens less than 1%. Perhaps the most convincing evidence is from the node 2 analysis. In 10,000 discriminant analyses separating *Pongo* from the hominines, all three specimens grouped with the latter in more than 90% of the replicates. This weighs heavily against the hypothesis that *Dryopithecus* shares supraorbital features with *Pongo* (Köhler et al., 2001). While it is clear that these data are robust for delineating orangutan morphology from that of the other apes, they do not reveal any similarities between *Dryopithecus* and *Pongo*.

Sivapithecus

Of the fossil specimens examined here, only GSP 15000 demonstrated strong affinities to *Pongo*. Curiously, this was not evident in scores from the first four eigenvectors. Indeed, this specimen was fairly unique on the first and third PCs (see Figures 2 and 3). Yet, in analyses designed to sort among known groups, it was well supported as a pongine; the whole-sample discriminant analysis grouped this fossil with *Pongo* at the highest probability, supported by 75% of the replicate assignments. These results bear particular significance in light of the highly autapomorphic nature of the orangutan brow (see Table 5). In node analyses, GSP 15000 showed a close affinity to *Pongo*, and secondarily to *Hylobates*. This statistically corroborates the consensus opinion about similarities between *Sivapithecus* and *Pongo*, and strongly supports a single character state for the two. Results from node 1, however, caution against drawing any further evolutionary significance from such analyses. In the shared features that distinguish extant hominids from hylobatids, GSP 15000 is demonstrably more like the latter. But, whether the node 1 and node 2 results represent

symplesiomorphy in *Sivapithecus*, autapomorphy in *Pongo*, or convergence in both cannot be ascertained from this study.

Figure 6c shows the landmark configuration of GSP 15000 superimposed over the shape differences between pongine and hominine brows (node 2). In nearly all aspects of the supraorbital morphology, *Sivapithecus* bears a strong similarity to the pongine configuration. Space curves in both are inferiorly placed in the midline, arch substantially, and terminate well superolateral to the hominine morphology. Mid-torus landmarks, especially in *Sivapithecus*, are medial to those of the hominine, reflecting the narrow interorbital breadth. The fronto-malar suture (FMT-FMO) in GSP 15000 and the pongine is broad medio-laterally with a strong supero-inferior component relative to the hominine; all three are similar in their antero-posterior dimension. The lateral view illustrates further similarities between the pongine and *Sivapithecus* morphology. Neither has a well-developed glabellar region, unlike the hominine configuration. And, the overall antero-posterior dimension of the brow is substantially reduced compared to the African apes and humans. This indicates a flatter morphology across the front of the upper face.

The analyses here were capable both of distinguishing *Pongo* from the other apes and of recognizing pongine affinities in an unknown specimen (GSP 15000). Orangutan features were noticeably absent from all other fossils. These results cannot preclude the argument that *Dryopithecus* and *Graecopithecus* were too primitive in pongine ancestry to exhibit many derived features (Köhler et al., 2001). They do suggest, however, that any such derived morphology is not present in the supraorbital region (*contra* Köhler et al., 2001).

Graecopithecus

Results for XIR 1 place it rather unambiguously with the hominines. In genus-level discriminant analyses, it was overwhelmingly linked to *Gorilla*. In node analyses, it grouped closely with hominids (89%) at node 1, and hominines at node 2 (96% vs *Pongo*, 89% vs *Hylobates*); these results strongly support hypotheses placing this morphology with the African apes and humans (Begun, 1992; Benefit and McCrossin, 1995). There is further evidence here linking XIR 1 to *Gorilla* (Dean and Delson, 1992), although support at node 3 (68%) was only moderate. As with *Dryopithecus*, there is no evidence to suggest pongine affinities. There is also no support here for a

Graecopithecus–Homo group (Bonis and Koufos, 2001); indeed, in genus-level replicate discriminations, XIR 1 grouped least-often with the modern human morphology.

Figure 6d depicts *Graecopithecus* superimposed over configurations representing the discrimination between *Gorilla* and the *Pan–Homo* clade. In frontal view, XIR 1 is similar to *Gorilla* in having a flatter space curve relative to rounded arch seen in *Pan–Homo*. Its overall contour, however, is not especially similar to either extant clade. *Graecopithecus* and *Gorilla* configurations are also broader than that of *Pan–Homo*, yet both have medially placed mid-torus landmarks; this indicates a narrower interorbital breadth compared to the hominins and chimpanzees. *Gorilla* and *Graecopithecus* also share broad lateral orbital pillars in medio-lateral and antero-posterior dimensions; in the supero-inferior dimension, however, the fossil specimen is greatly reduced relative to both groups. In lateral view, XIR 1 tends to mimic the *Gorilla* morphology except at glabella and nasion (NAS). The marked inferior displacement of nasion in *Graecopithecus* resembles neither extant morphology. While the overall supraorbital morphology of *Graecopithecus* is more similar to *Gorilla* than to the *Pan–Homo* group, in many features it appears to be fairly unique.

CONCLUSIONS

This project used three-dimensional landmark-based morphometric analyses to quantify morphology and variation in the supraorbital region of extant and fossil hominoids. Based on Procrustes superimposition and a battery of statistical approaches, several results were obtained. First, it was demonstrated that supraorbital morphology is robust for distinguishing among extant hominoids. Three character states are exhibited in living apes, separating hominines, *Pongo*, and *Hylobates*; *Homo* is best placed with the African apes in brow morphology, rather than in a separate category. Second, Late Miocene hominoid specimens of *Dryopithecus*, *Sivapithecus*, and *Graecopithecus* were shown to have affinities with particular branches of the hominoid phylogeny. *Dryopithecus* from Hungary best represents stem hominid morphology; *Dryopithecus* from Spain is fairly unique, with uncertain affinities. *Sivapithecus* shows strong affinities to *Pongo* and the pongine lineage, but displays some similarity to hylobatids. Finally, *Graecopithecus* clearly groups with the hominines, and shows some affinity to the *Gorilla* lineage.

ACKNOWLEDGMENTS

I thank Dr. Slice for organizing the AAPA morphometrics symposium, for inviting me to participate in this volume, and especially for the help he has given me and other morphometricians around the world. I am grateful to all those who provided access to specimens in their care: Bob Randall, Ross MacPhee, Richard Thorington, Linda Gordon, Judith Chupasko, David Pilbeam, John Harrison, Malcolm Harman, Manfred Ade, Wim Van Neer, László Kordos, David Begun, and Jay Kelley. I especially thank Eric Delson, Terry Harrison, David Begun, Michelle Singleton, Jim Rohlf, Steve Frost, and Katerina Harvati for their support in this and many other endeavors, as well as Suzanne Hagell and Karen Baab for real-time solutions. Finally, many thanks to the late Dr. Leslie Marcus for bringing life, laughter, and enlightenment to the world of morphometrics. This project was undertaken as part of my dissertation work at the City University of New York, supported by the New York Consortium in Evolutionary Primatology and American Museum of Natural History, and partially funded by NSF grants to NYCEP (DBI 9602234) and the NYCEP Morphometrics Group (ACI 9982351). This is NYCEP Morphometrics contribution number nine.

REFERENCES

Andrews, P., 1992, Evolution and the environment in the Hominoidea, *Nature* 360:641–646.

Begun, D. R., 1992, Miocene fossil hominoids and the chimp-human clade, *Science* 257:1929–1933.

Begun, D. R., 1994, Relations among the great apes and humans: New interpretations based on the fossil great ape *Dryopithecus, Yearb. Phys. Anthropol.* 37:11–63.

Begun, D. R. and Moyà Solà, S., 1992, A new partial cranium of *Dryopithecus laietanus* from Can Llobateres, *Am. J. Phys. Anthropol.* (Suppl.) 14:47.

Begun, D. R., Ward, C. V., and Rose, M. D., 1997, Events in hominoid evolution, in: *Function, Phylogeny, and Fossils. Miocene Hominoid Evolution and Adaptations*, D. R. Begun, C. V. Ward, and M. D. Rose, eds., Plenum Press, New York, pp. 389–416.

Benefit, B. R. and McCrossin, M. L., 1995, Miocene hominoids and hominid origins, *Annu. Rev. Anthropol.* 24:237–256.

Bonis, L., de and Koufos, G. D., 2001, Phylogenetic relationships of *Ouranopithecus macedoniensis* (Mammalia, Primates, Hominoidea, Hominidae) of the late Miocene

deposits of central Macedonia (Greece), in: *Phylogeny of the Neogene Hominoid Primates of Eurasia*, L. de Bonis, G. D. Koufos, and P. Andrews, eds., Cambridge University Press, Cambridge, pp. 254–268.

Bookstein, F. L., Schäfer, K., Prossinger, H., Fieder, M., Stringer, C. Weber, G. et al., 1999, Comparison of frontal cranial profiles in archaic and modern *Homo* by morphometric analysis, *Anat. Rec. (The New Anatomist)* 257:217–224.

Cameron, D. W., 1999, The single species hypothesis and *Hispanopithecus* fossils from the Vallés Penedés basin, Spain, *Z. Morph. Anthropol.* 82:159–186.

Collard, M. and Wood, B., 2000, How reliable are human phylogenetic hypotheses? *PNAS* 97:5003–5006.

Dean, D., 1993, The middle Pleistocene *Homo erectus/Homo sapiens* transition: New evidence from space curve statistics, Unpublished Ph.D. Dissertation, Department Anthropology, City University of New York.

Dean, D. and Delson, E., 1992, Second gorilla or third chimp? *Nature* 359:676–677.

Dean, D., Marcus, L. F., and Bookstein, F. L., 1996, Chi-square test of biological space curve affinities, in: *Advances in Morphometrics, NATO ASI Series*, L. F. Marcus, M. Corti, A. Loy, G. J. P. Naylor, and D. E. Slice, eds., Plenum Press, New York, pp. 235–251.

Dryden, I. L. and Mardia, K. V., 1998, *Statistical Shape Analysis*, John Wiley, New York.

Harvati, K., 2001, The Neanderthal problem: 3-D geometric morphometric models of cranial shape variation within and among species, Unpublished Ph.D. Dissertation, Department Anthropology, City University of New York.

Köhler, M., Moyà Solà, S., and Alba, D. M., 2001, Eurasian hominoid evolution in the light of recent *Dryopithecus* findings, in: *Phylogeny of the Neogene Hominoid Primates of Eurasia*, L., de Bonis, G. D. Koufos, and P. Andrews, eds., Cambridge University Press, Cambridge, pp. 192–212.

Kordos, L., 1987, Description and reconstruction of the skull of *Rudapithecus hungaricus* Kretzoi (Mammalia), *Ann. Hist. Natur. Mus. Nat. Hung.* 79:77–88.

Kordos, L. and Begun, D. R., 2001, A new cranium of *Dryopithecus* from Rudabáya, Hungary, *J. Hum. Evol.* 41:689–700.

Marcus, L. F., 1969, Measurement of selection using distance statistics in the prehistoric orang-utan *Pongo pygmaeus paleosumatrensis*, *Evolution* 23(2):301–307.

Marshall, J. and Sugardjito, J., 1986, Gibbon systematics, in: *Comparative Primate Biology, Volume 1: Systematics, Evolution, and Anatomy*, D. R. Swindler and J. Erwin, eds., Alan R. Liss, New York, pp. 137–185.

McNulty, K. P., 2003, Geometric morphometric analyses of extant and fossil hominoid craniofacial morphology, Unpublished Ph.D. Dissertation, Department Anthropology, City University of New York.

Moyà Solà, S. and Köhler, M., 1995, New partial cranium of *Dryopithecus* lartet, 1863 (Hominoidea, Primates) from the upper Miocene of Can Llobateres, Barcelona, Spain, *J. Hum. Evol.* 29:101–139.

Neff, N. A. and Marcus, L. F., 1980, A survey of multivariate methods for systematics. Numerical Methods in Systematic Mammalogy Workshop, American Society of Mammalogists.

O'Higgins, P. and Jones, N., 1998, Facial growth in *Cercocebus torquatus*: an application of three-dimensional geometric morphometric techniques to the study of morphological variation, *J. Anat.* 193:251–272.

Pilbeam, D. R. and Young, N. M., 2001, *Sivapithecus* and hominoid evolution: Some brief comments, in: *Hominoid Evolution and Climate Change in Europe, Volume 2: Phylogeny of the Neogene Hominoid Primates of Eurasia*, L. de Bonis, G. D. Koufos, and P. Andrews, eds., Cambridge University Press, Cambridge, pp. 349–364.

Rohlf, F. J., 1999, *tpsSmall* v. 1.17, Department of Ecology and Evolution, State University of New York, Stony Brook, New York.

Rohlf, F. J. and Marcus, L. F., 1993, A revolution in morphometrics, *Trends Evol. Ecol.* 8:129–132.

Ruvolo, M., 1994, Molecular evolutionary processes and conflicting gene trees: The hominoid case, *Am. J. Phys. Anthropol.* 94:89–114.

Schwartz, J. H., 1987, *The Red Ape. Orang-utans and Human Origins*, Houghton Mifflin Company, Boston.

Slice, D. E., 1998, *Morpheus et al.: Software for Morphometric Research*, Department of Ecology and Evolution, State University of New York, Stony Brook, New York.

Slice, D. E., 2001, Landmark coordinates aligned by Procrustes analysis do not lie in Kendall's shape space, *Syst. Biol.* 50:141–149.

Slice, D. E., Bookstein, F. L., Marcus, L. F., and Rohlf, F. J., 1996, Appendix I—a glossary for geometric morphometrics, in: *Advances in Morphometrics*, L. F. Marcus, M. Corti, A. Loy, G. J. P. Naylor, and D. E. Slice, eds., Plenum Press, New York, pp. 531–551.

Ward, S. C. and Kimbel, W. H., 1983, Subnasal alveolar morphology and the systematic position of *Sivapithecus*, *Am. J. Phys. Anthropol.* 61:157–171.